CHAPTER 1: Introduction

1.1 Encapsulation in Endohedral Fullerene

Spatial confinement of atoms and molecules has been an exciting and active area of research in physical sciences. Many models have been used to describe confinement. Particle in a one-dimensional box and spherical cage are the simplest examples. The cages are like potential wells, where a species once trapped inside has to cross a certain potential barrier to come out. Many molecules have been discovered, which are hollow cages and can entrap guest species. Chemical species encapsulated by carbon clusters have become a paradigm of confined systems. Among all carbon cage molecules, fullerenes are the most investigated. The discovery of fullerene led to its discoverers, Kroto, Smalley and Curl win the Chemistry Nobel Prize in 1991. Kroto was originally interested in the formation of interstellar long carbon chains, HC_5N, HC_7N, and HC_9N in red giant stars, but encountered unexpected molecules which contradicted the traditional wisdom that only two allotropes of carbon existed, namely graphite and diamond. The unexpected molecules discovered by Kroto and collaborators were fullerenes, which are now considered as the third allotrope of carbon. Fullerenes are denoted by C_m, where *m* refers to the number of carbon atoms in the molecule. Among all the C_m molecules synthesized in the reaction by Kroto, C_{60} happens to be the most common one. The name fullerene was christened to this molecule to pay credit to R. Buckminster Fuller for his novel geodesic "soccer ball" structure similar to what was built in Montreal, Canada (see Figure 1.1).

Figure 1.1: Group photograph of Kroto and collaborators and Buckminster Fuller and the dome in Montreal, Canada

The C_{60} fullerene has empty space inside that can encapsulate atoms and molecules. The resulting complexes are called endohedral fullerenes and are represented by $X@C_{60}$, where *X* refers to the guest atom or molecule. The first experimental realization of endohedral fullerenes came soon after the discovery of fullerene. Synthesis of La@ C_{60} by laser vaporization of graphite intercalated with $LaCl_3$ was announced for the first time by Heath et al [1]. Figure 1.2 shows the structure of an endohedral fullerene, $X@C_{60}$.

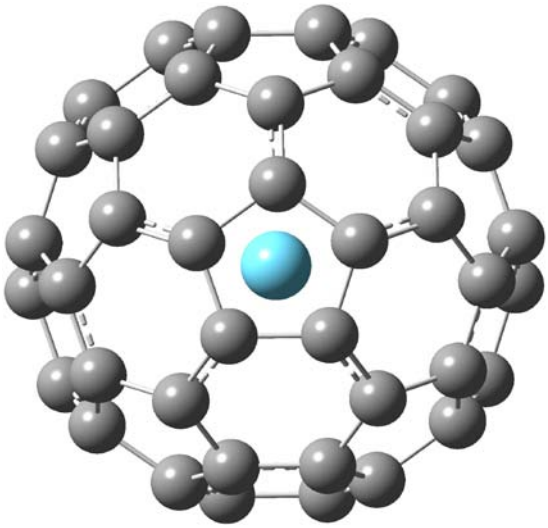

Figure 1.2: Schematic representation of an endohedral fullerene $X@C_{60}$

Since then several methods have been developed to make endohedral fullerenes having different guest species. Laser vaporization of graphite sheet intercalated with metal salts [2] and high energy collision between the guest species and host fullerene cage are some of the early methods. Recently, a novel molecular surgery method was developed [3] to encapsulate guest species. As the name suggests, the method involves molecular surgery, which consists of three steps: opening the fullerene molecule by a chemical reaction, inserting the guest species and stitching the opened structure to get back the original framework. This method is illustrated in Figure 1.3. Analytical tools like ultraviolet-visible absorption spectroscopy, nuclear magnetic resonance spectroscopy (NMR) and electron spin resonance (ESR) are widely used for structural elucidation and characterization of these endohedral fullerene molecules. A lot of experimental and theoretical research has been performed in the field of endohedral chemistry for the last two decades. In this thesis project, only a theoretical study of certain endohedral fullerenes was done.

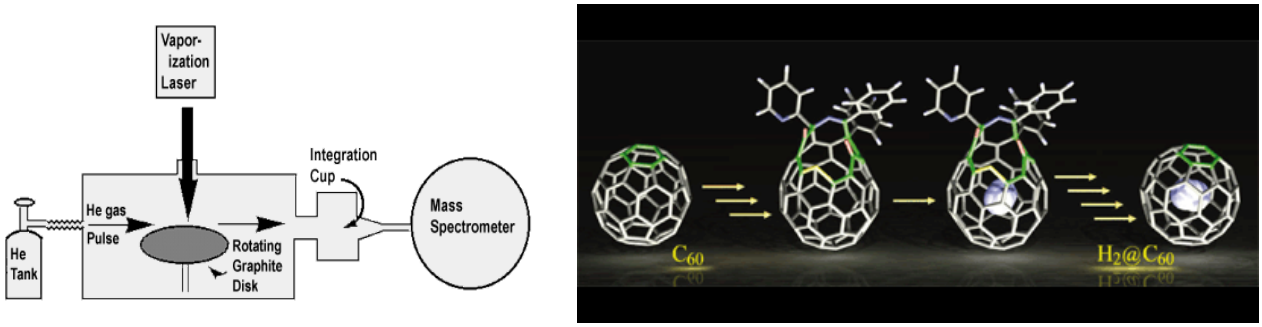

Figure 1.3: Schematic diagram of the experimental setup for Laser vaporization coupled with mass spectrometer in the left panel and illustration of the molecular surgery method [3] in the right panel.

Endohedral fullerenes are of immense practical interest since confinement of a guest species inside fullerene can tune the electronic structure, energy gap, physical and chemical properties of both the host (fullerene), and the guest species. Many theoretical and experimental investigations have been carried out to decipher different effects of confinement. The pioneering work of a theoretical investigation of endohedral complexes of fullerene was done by Cioslowski et al. [4]. They investigated iso-electronic F^-, Ne, Na^+, Mg^{2+} and Al^{3+} species inside C_{60} cage and showed that in the stable form the species are located at the centre of the cage. An expansion of the cage in presence of cationic guest species and a contraction for anionic guest species was also elucidated by them. Ramachandran et al. [5] studied the interaction of H^+, H^-, He, Li^+ and H_2 with C_{60} cage using Hartree-Fock and second order Moller-Plesset perturbation (MP2) theory.

The barrier for penetration of the guest species through the centre of a hexagonal ring of the cage reported by them is illustrated in the Figure 1.4. From the figure, it can be concluded that H^+ and Li^+ ions form endohedral as well as exhohedral complexes with the C_{60} cage. In exohedral complexes, interaction of a chemical species with the (fullerene) cage is from outside whereas in endohedral complexes, small molecules or atoms get trapped inside the fullerene cage.

The structure and stability of nitrogen, phosphorous and lithium encapsulated in C_{60} has also been studied [6-7]. The study by Bukingham and Read attributed the stability of Li in an eccentric position of C_{60} to the lifting of degeneracy of the molecular orbitals [8]. Gadolinium encapsulated fullerene derivatives have been reported to be a good contrasting agent in magnetic resonance imaging. It has been shown that the most stable structure of $Gd@C_{60}$ has Gd located symmetrically with respect to one of the hexagonal rings. Population analysis suggested the oxidation state of the encapsulated Gd to be +3 [9].

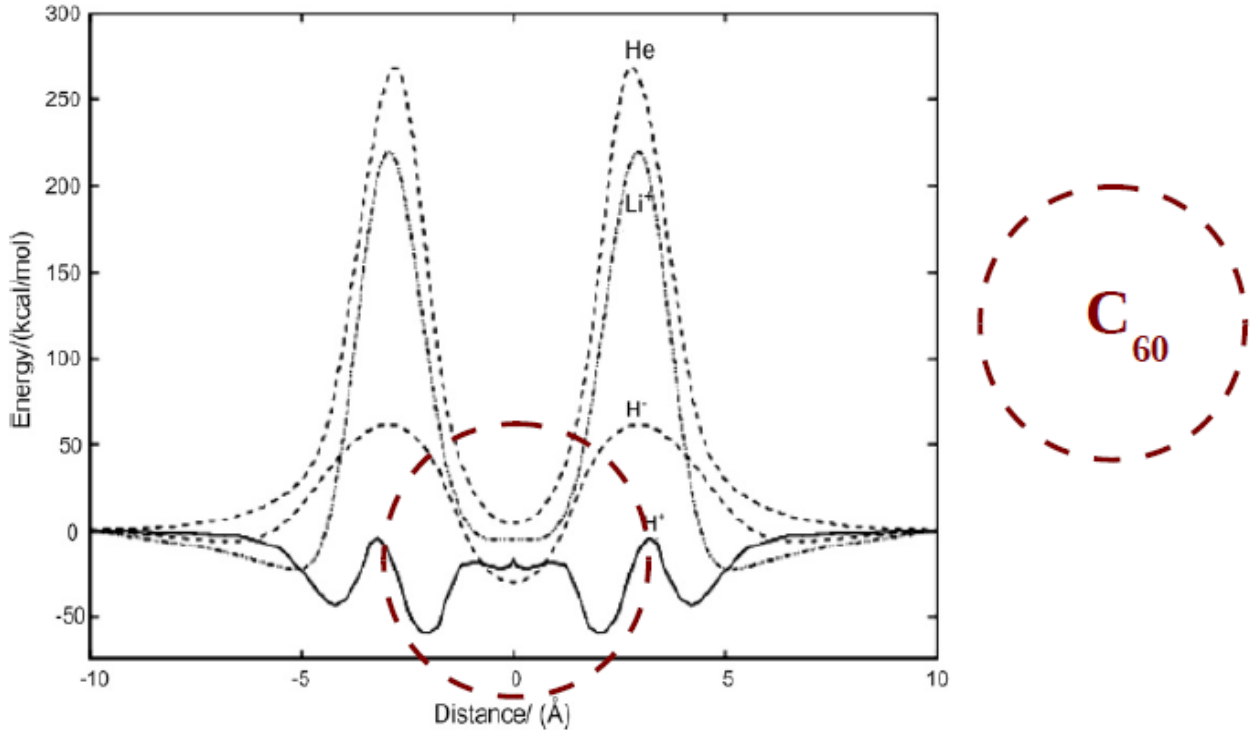

Figure 1.4: The ground state interaction potential for the guest species (H^+, H^-, Li^+, He) approaching C_{60} through the centre of a hexagonal ring.

Cioslowski et al. carried out Hatree-Fock calculation to study the encapsulation of small diatomic molecules and showed that the C_{60} cage acts as a polarisable sphere, thus stabilizing polar molecules and destabilizing nonpolar molecules. The rotational motion of H_2 inside C_{60} was examined by Cross [10]. A small torque on H_2 is reported, when it is in an off-centre position. Other significant research in endohedral fullerene chemistry includes the work done by Zicovich [11]. He investigated the spatial confinement of simple quantum mechanical systems in microscopic spherical and cubic potential wells. Based on their model, they predicted a decrease in the energy gap between the highest occupied molecular orbital (HOMO) and the lowest unoccupied molecular orbital (LUMO) of spatially confined ethylene [12]. In many studies, the altered energy spectra of the host and the guest after confinement have been reported although this result cannot be generalized. Changes in the energy levels also change the optical properties of the host and the guest. Trimetallic nitride endohedral C_{60} fullerenes, TNEFs, have been sought for their unique opto-electronic properties [13]. Shameema et al. [15] studied the encapsulation of iso-electronic molecules HF, H_2O, NH_3 and CH_4 and reported a blue shift in the stretching frequencies of the guest molecules due to confinement. Ramachandran and Sathyamurthy [16] studied the structure

and stability of water clusters confined inside the C_{60} fullerene cage. It was shown that encapsulation results in the breaking of hydrogen bonds between water molecules and change in the shape of water clusters. It was reported that $(H_2O)_4$ inside the C_{60} cage is tetrahedral in arrangement, in contrast to a square planar geometry observed in the gas phase.

1.2 Computational Method

There are different computational methods available to determine the structure of a molecular system and predict its properties. They can be classified as molecular mechanics methods, ab initio quantum mechanical methods and density functional methods.

Molecular mechanics, also called the force-field method, uses classical mechanics to predict the energy of a molecule as a function of its molecular geometry. In molecular mechanics, the total potential energy is expressed as a sum of Taylor series expansions for stretches in every pair of bonded atoms, and additional terms coming from bending, torsional energy, van der Waals interaction, electrostatics, and cross terms [17]:

$$E = E_{str} + E_{bend} + E_{tors} + E_{vdw} + E_{el} + E_{cross.} \quad (i)$$

These methods predict equilibrium geometries, transition states and relative energies between conformers of a molecule. They are mostly used for calculating the potential energy for molecular dynamics simulations for large molecules.

The most popular *ab initio* electronic structure methods are Hartree–Fock and Post-Hartree–Fock methods. The former, perhaps the simplest type of an ab initio method is based on variational theory. It includes restricted open-shell Hartree–Fock (RHF) and unrestricted Hartree–Fock (UHF) methods. The main drawback of this method is that the instantaneous electron-electron correlation is not specifically taken into account. Post-Hartree–Fock methods begin invaribaly with a Hatree-Fock calculation and proceed to correct for the electron correlation. Post-Hartree–Fock methods include n^{th} order Møller–Plesset perturbation theory (MPn), Configuration interaction (CI), Coupled cluster (CC) and related methods [17].

In some cases, where the Hartree–Fock method is inadequate and a single-determinant reference function is not a good basis for post-Hartree–Fock methods, multi-determinant references are used

for an improvement. Such multi-reference methods are multi-configurational self-consistent field (MCSCF), multi-reference configuration interaction (MRCI), n-electron valence state perturbation theory (NEVPT) and n^{th} order complete active space perturbation theory (CASPTn).

Density Functional theory (DFT) is the most commonly used method to calculate the electronic structure and properties of chemical compounds. It is based on the theorem proved in 1964 by Hohenberg and Kohn that states that the energy (*Eg*) and all other properties of a ground state molecule can be uniquely determined by the ground state electron probability density (*p*). In 1965, Kohn and Sham devised a practical method to determine *p* and then subsequently find *Eg* from *p*. This work earned Kohn the 1998 Nobel Prize in chemistry. Various types of DFT functionals have been proposed over the years. They include the Local Density Approximation (LDA) functional, Generalized Gradient corrected functionals like Becke gradient-exchange correlation and Lee-Yang-Parr correlation functional (BLYP), hybrid functionals like Beke-3parameter-Lee-Yang-Parr (B3LYP) functional and meta hybrid functionals like the M06 [17].

1.3 Structure of C_{60}

A fullerene molecule consists of 12 pentagonal and 20 hexagonal rings. The pentagonal rings give a three dimensional structure to the cage. The spherical cage would not have been possible, but not for the pentagonal rings. This is illustrated in the Figure 1.5. The stability of the cage is determined by an empirical rule called the isolated pentagon rule (IPR). According to IPR [18], a spherical fullerene cage will not have any two pentagonal rings fused together. C_{60} is the smallest fullerene molecule possible in which the pentagonal rings are isolated from each other.

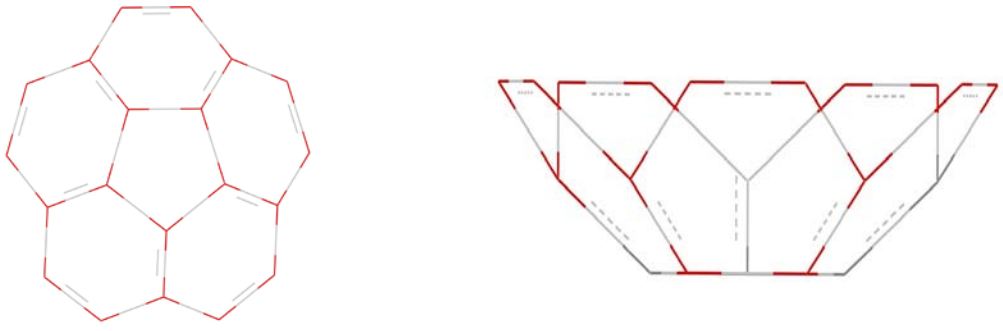

(a) Top View (b) Side View

Figure 1.5: (a) Top view of a pentagon surrounded by five hexagons and (b) side view of the same

Fullerene comprises of 90 covalent bonds, among which 60 are single bonds and 30 are double bonds. The hexagonal rings have two types of bonds: a shorter (6-6) bond shared by two consecutive hexagonal rings and a longer (5-6) bond shared by adjoining hexagonal and pentagonal rings. At the HF/ccpVDZ level of calculation, the (6-6) bond length is 1.38 Å and the (5-6) bond length is 1.46 Å. These values are in agreement with the reported neutron diffraction measurements [19] of 1.39 and 1.46 Å, respectively. These values fall between the C-C (1.53 Å) and C=C (1.32 Å) bond lengths. The hexagonal rings have unsaturated carbons and are slightly aromatic, but much less aromatic than the planar benzene ring. It should be noted that the carbon atoms in C_{60} are not exactly sp^2 hybridized. The reason for this is that all these sp^2 hybrid orbitals of an atom lie in the same plane but C_{60} is not planar and the environment of each carbon cannot be planar. All the carbon atoms in C_{60} are equivalent and this is validated by a single peak in the NMR spectrum (see Figure 1.6) of this molecule [20].

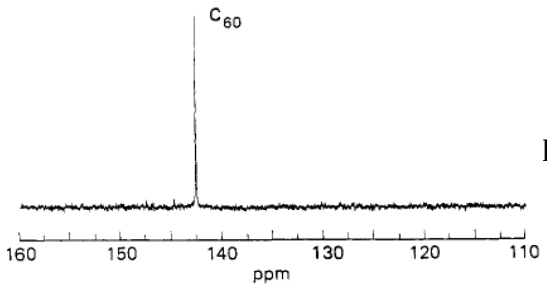

Figure 1.6: ^{13}CNMR spectra of C_{60}. The resonance peak at 142.5 ppm is assigned to C_{60} [20].

It should be emphasized that the C_{60} molecule is not exactly spherical, but rather like a truncated icosahedral. If C_{60} was spherical, then the solution to the Schrödinger's equation for a particle on a sphere would predict the molecule to be paramagnetic, with 10 unpaired electrons [17]. This would suggest that C_{60} is perhaps a conductor of electricity. In fact C_{60} is diamagnetic with no unpaired electrons and it does not conduct electricity. However, lower symmetry point group and truncated icosahedron predict a fully filled penta-degenerate as the highest occupied molecular orbital for C_{60}. Its structure is shown in Figure 1.7.

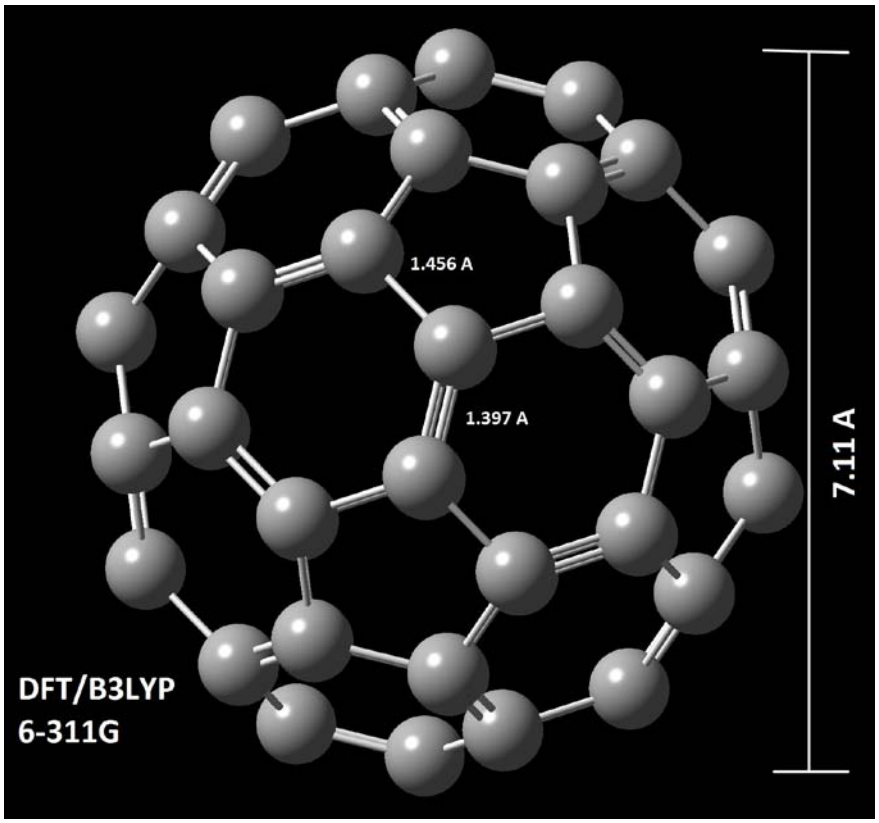

Figure 1.7: C_{60} optimized structure

CHAPTER 2: Change in magnetic properties of diatomic species upon encapsulation

2.1

Encapsulation can also alter the magnetic properties of the guest molecules. The effect of confinement by carbon cage on size dependent magnetic properties of Ni nanoparticles studied by Ang et al. [21] led to the conclusion that the diamagnetic contribution of the carbon cage reduces the magnetic moment of the core, an effect more prominent as the particle size decreases. Experimental studies of magnetic properties of confined materials, using electron spin resonance (ESR) have produced striking results. ESR spectra of $Sc@C_{82}$, $Y@C_{82}$ and $La@C_{82}$ manifest hyperfine splitting caused by the interaction of unpaired electrons on the C cage with the nuclear spin of the metal ion in the endohedral complex. Muller et al. [22] in their experimental investigation reported that contrary to $Sc@C_{82}$, $Y@C_{82}$ and $La@C_{82}$, endohedral complexes of Eu, Gd, Tm and Yb did not show the hyperfine structure in the ESR signal. A probable reason for the missing ESR spectra may be an even number of positive charges at the metal ion inside the cage and zero unpaired electrons on the fullerene cage. Thus, the difference in behaviour is caused by the magnitude of charge at the metal ion and the counter ionic state of the carbon cage. Magnetic anisotropy of endohedral metallofullerenes and multi-walled carbon nanotubes (MWCNTS) has been studied using superconducting quantum interface device (SQUID) magnetometer. Studies [23] support that atoms and molecules entrapped inside single walled carbon nano tubes (SWCNTs) and MWCNTs also manifest unusual properties.

Paramagnetic endohedral fullerenes ($M@C_n$), compounds that contain a paramagnetic species (M) inside the fullerene cage (C_n) hold much promise as the basic elements for realizing nanometer scale devices such as molecular magnets, superconductors with low critical temperatures, field effect transistors, quantum dots and fullerene-based quantum computers. Production of giant magneto-resistance wires (GMR) by incorporating carbon encapsulated cobalt nanoparticles has also been reported [24]. Gadolinium-filled endohedral metallofullerenes are potentially effective as new magnetic resonance imaging contrast agents [25]. Magnetic substances confined by the carbon cage have received considerable attention because of their potential to be used also as novel data storage materials. Ferromagnetic nanoclusters are very useful for magnetic recording. However, application of ferromagnetic nanoclusters is limited due to air-oxidation. Encapsulation of these

materials within inert materials can prevent air oxidation thus allowing them to sustain magnetic properties for a longer time. Lee et al. [26] have reported that nickel as well as cobalt nanoclusters encapsulated by fullerene possess excellent magnetic properties.

The study by Koltover [27] has revealed that in paramagnetic endo-metallofullerenes ($M@C_{2n}$), there is a partial runoff of electron spin density outside the fullerene cage ("spin leakage"), which has been testified by electron paramagnetic resonance and nuclear magnetic resonance data. On the other hand, in paramagnetic $N@C_{60}$ and $P@C_{60}$, there is an accumulation of electron spin density on the entrapped atoms seemingly as if the electronic shells of the entrapped atoms are compressed ("spin compression").

Despite of having tremendous potential as novel materials, the effect of confinement by carbon cages on magnetic properties of guest species is still not well understood. The motive of this thesis project is to reflect the change in the magnetic behaviour/properties of a diatomic molecule, X_2 encapsulated in C_{60} with respect to free X_2 molecules. No such study has not yet been done till this date to the best of our knowledge.

Considering the size of the cavity inside the C_{60} fullerene, it may be possible to encapsulate diatomic molecules like B_2, O_2 and Ge_2. However there is no experimental evidence for such an encapsulation, as of now. Krap and Frenking [28] have studied theoretically the possibility of encapsulation of dimers of rare gas atoms inside C_{60}. Their DFT and MP2 calculations using different basis sets showed that it is possible to trap these species inside C_{60}. Encapsulation of U_2 has also been reported both experimentally and theoretically [29]. In this section theoretical investigations have been carried out to check the possibility of encapsulation of B_2, O_2 and Ge_2 in C_{60} in singlet and triplet states using different methods and basis sets.

2.2 Computational Details

Geometry optimization and vibrational frequency calculations for all the $X_2@C_{60}$systems were carried out using Gaussian09 suite of programs at the IISER Mohali computational facility centre. The calculations were done using different ab initio methods including UHF (for triplet state), RHF and density functional M06L, M06-2X and b3pw91. Different basis sets including 6-31G, 6-311G(d), cc-pVDZ and cc-pVTZ were used. Frequencies were calculated at the same level of theory to distinguish the saddle points and minima energy conformers. Natural bond analysis

(NBO) was also carried out to get a better insight of the dispersion interaction between the guest species and the host cage. All the stabilization energy values were calculated by the supermolecule approach as follows:

$$E_{stab} = E_{complex} - (E_{C60} + E_{guest}). \quad (ii)$$

2.3 Results and Discussion

2.3.1. Bond parameters and relative energy of free diatomic molecules

Free B_2, O_2 and Ge_2 are triplets in their ground electronic state. At the HF/6-311G(d) level of calculation, the B_2 triplet is more stable than B_2 singlet by an energy of 30.59 kcal/mol, while DFT methods predict the triplet state to be around 23 kcal/mol lower in energy than the singlet. At all levels of calculation the bond lengths of triplet and singlet B_2 are almost the same. O_2 triplet is more stable than O_2 singlet by an energy of 53.28 kcal/mol at HF/6-311G(d) level of calculation, while in the DFT methods, the relative stability of triplet state over singlet state varies between 37 to 42 kcal/mol, depending upon the density functional used. At all levels of calculation the bond lengths of triplet and singlet O_2 are the same, just as in B_2. Similar calculations show that Ge_2 triplet is more stable than Ge_2 singlet by 22.48 kcal/mol at the HF/6-311G(d) level of theory. At DFT methods, the relative stability of triplet is around 18 kcal/mol. Tables 1, 2 and 3 give the relative energies of the triplet states over the singlet states at different level of calculations. The tables also give the bond lengths of the diatomic molecules. The experimental bond lengths of B_2, O_2 and Ge_2 are 1.590 Å, 1.204 Å and 2.52 Å respectively [30,31].

Table 2.1: Relative energy (in kcal/mol) of B_2 (triplet) with respect to B_2 (singlet) and the B_2 bond length (in Å) in the singlet and triplet states.

Method	Basis Set	Bond Length (Singlet)	Bond Length (Tripet)	$E_{(Triplet-Singlet)}$
HF	6-311G(d)	1.68	1.64	-30.59
B3Pw91	6-311G(d)	1.64	1.62	-24.33
M06-2X	6-311G(d)	1.65	1.62	-22.01
M06-L	6-311G(d)	1.64	1.61	-23.92

Table 2.2: Relative energy (in kcal/mol) of O_2 (triplet) with respect to O_2 (singlet) and O_2 bond length (in Å) in the singlet and triplet states

Method	Basis Set	Bond Length (Singlet)	Bond Length (Tripet)	$E_{(Triplet-Singlet)}$
HF	6-311G(d)	1.15	1.15	-53.28
B3Pw91	6-311G(d)	1.20	1.20	-40.22
M06-2X	6-311G(d)	1.19	1.19	-37.65
M06-L	6-311G(d)	1.19	1..20	-41.45

Table 2.3: Relative energy (in kcal/mol) of Ge_2 (triplet) with respect to Ge_2 (singlet) and Ge_2 bond length (in Å) in the singlet and triplet states

Method	Basis Set	Bond Length (Singlet)	Bond Length (Tripet)	$E_{(Triplet-Singlet)}$
HF	6-311G	2.42	2.39	-22.48
	6-311G(d)	2.39	2.35	-25.35
B3Pw91	6-311G(d)	2.42	2.39	-18.26
M06-2X	6-311G(d)	2.41	2.40	-20.33
	cc-pvtz	2.41	2.38	-19.38
M06-L	6-311G(d)	2.41	2.40	-17.10
	cc-pvtz	2.41	2.40	-16.24

2.3.2 Encapsulation of X_2@C60

O_2 has the shortest bond length and Ge_2 has the longest bond length among all the three paramagnetic diatomic molecules considered for this project. As mentioned in the table 1, 2 and 3, the bond length of O_2 (triplet), B_2 (triplet) and Ge_2 (triplet) are 1.19 Å, 1.61 Å and 2.40 Å respectively at M06-L level of theory. When these molecules are encapsulated by C_{60}, Ge_2 being the longest will be the closest to the inner surface of C_{60}, while the shortest molecule O_2 will be farthest

from the inner surface of C_{60}. Upon encapsulation, the distance between Ge_2 and fullerene inner wall will be ~ 0.4 Å, whereas O_2 will ~ 1.7 Å away from fullerene inner wall. This is illustrated in the Figure 2.1.

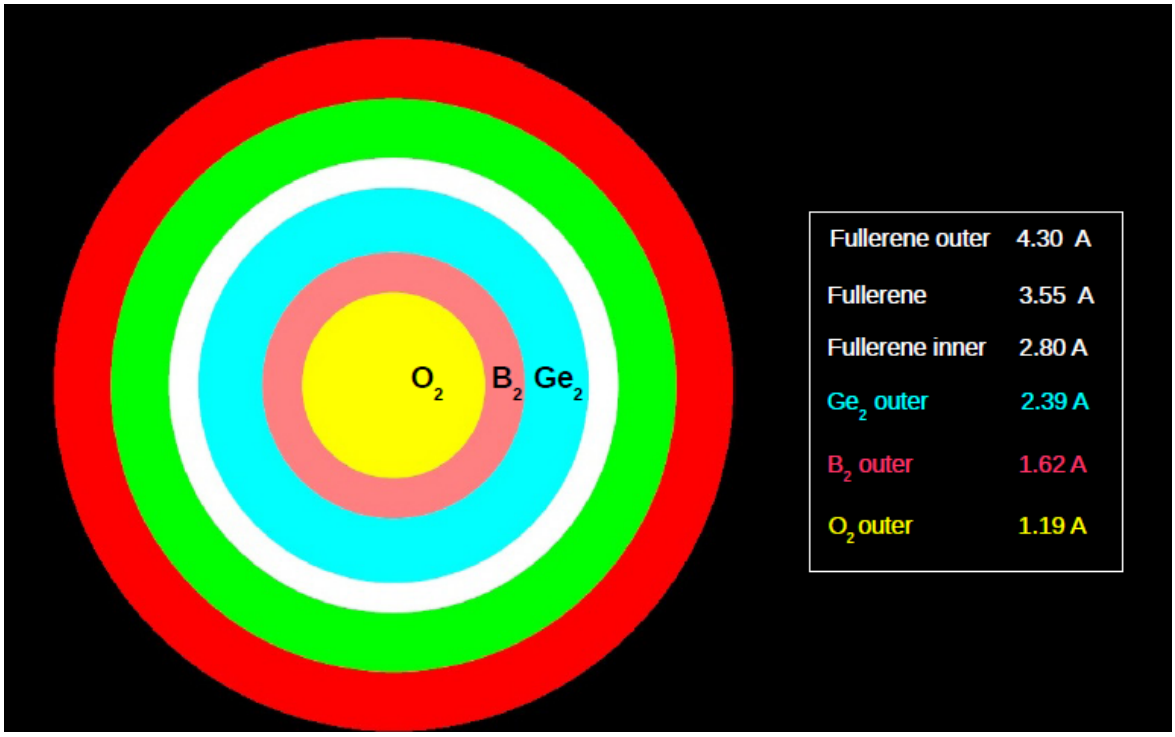

Figure 2.1: Schematic representation of the size of different diatomic molecules inside fullerene cage

Since the pi-electron density is not uniform on the surface of C_{60}, we expect that the interaction of endohedral guest species with the fullerene cage will be orientation dependent. There are many different orientations possible for an X_2 molecule encapsulated in C_{60}. The X_2 molecule oriented along the line joining the centres of two opposite pentagonal rings and its centre of mass coinciding with the centre of a fullerene molecule will have the highest symmetry possible for an $X_2@C_{60}$ complex. Such a molecule will belong to the D_{5d} point group. When the X_2 molecule is oriented along the line joining the centres of two opposite hexagons, the complex will have a C_3 rotation axis and will belong to the D_{3d} point group. X_2 pointing towards the centre of C_{hex}- C_{hex} bond will belong to the D_{2h} point group, while orientation towards the centre of C_{hex}- C_{pent} bond will make it belong to the C_{2h} point group. These four different orientations are illustrated in the Figure 2.2.

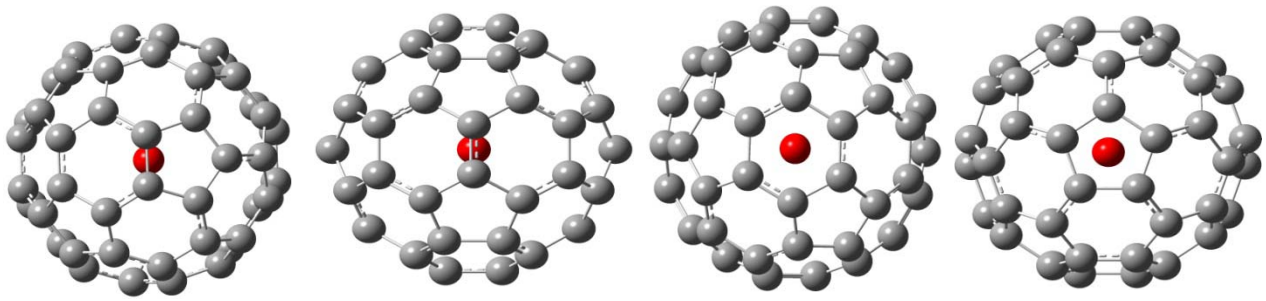

C_{2h} D_{2h} D_{3d} D_{5d}

Figure 2.2: Different possible symmetry groups for $X_2@C_{60}$

2.3.3 Stabilization energy for different complexes at different angles and different methods

Stabilization energy values were calculated for B_2, O_2 and Ge_2 encapsulated in C_{60} along different orientations. BSSE corrections were not done while calculating stabilization energy values. The results, relative to the energy of fullerene and triplet X_2 molecules are listed in the tables 2.4-2.9.

Table 2.4: Stabilization energy (in kcal/mol) of $B_2@C_{60}$ (singlet) with respect to B_2 (triplet) and C_{60}

Method	Basis Set	D_{5d}	D_{3d}	D_{2h}	C_{2h}
HF	6-311G(d)	72.54	72.44	72.48	72.45
B3Pw91	6-311G(d)	35.29	35.00	35.03	35.18
M06-2X	6-311G(d)	7.84	7.84	7.80	7.78
M06-L	6-311G(d)	9.18	9.21	9.25	9.28

Table 2.5: Stabilization energy (in kcal/mol) of $B_2@C_{60}$ (triplet) with respect to B_2 (triplet) and C_{60}

Method	Basis Set	D_{5d}	D_{3d}	D_{2h}	C_{2h}
HF	6-311G(d)	40.91	40.85	40.86	40.88
B3Pw91	6-311G(d)	11.34	11.05	11.11	11.11
M06-2X	6-311G(d)	-20.05	-20.40	-20.28	-20.39
M06-L	6-311G(d)	-20.07	-19.72	-19.69	-19.98

From the Tables 2.4 and 2.5, we conclude that at the HF level of theory, encapsulation of B_2 in C_{60} is endothermic. Calculations at the DFT/M06-L and DFT/M06-2X level, however, suggest that the encapsulation of B_2 (triplet) inside C_{60} giving $B_2@C_{60}$ (triplet) is energetically favourable while the formation of $B_2@C_{60}$ (singlet) is an endothermic process.

Table 2.6: Stabilization energy (in kcal/mol) of $O_2@C_{60}$ (singlet) with respect to O_2 (triplet) and C_{60}

Method	Basis Set	D_{5d}	D_{3d}	D_{2h}	C_{2h}
HF	6-311G(d)	59.89	59.86	59.89	59.89
B3Pw91	6-311G(d)	42.87	43.17	43.44	43.40
M06-2X	6-311G(d)	16.92	17.56	18.11	16.96

Table 2.7: Stabilization energy (in kcal/mol) of $O_2@C_{60}$ (triplet) with respect to O_2 (triplet) and C_{60}

Method	Basis Set	D_{5d}	D_{3d}	D_{2h}	C_{2h}
HF	6-311G(d)	6.91	6.88	6.88	6.89
B3Pw91	6-311G(d)	4.14	3.96	4.14	4.31
M06-2X	6-311G(d)	-20.43	-20.00	-19.62	-20.08

Table 2.6 suggests that at all level of calculations, encapsulation of O_2 triplet giving rise to $O_2@C_{60}$ (singlet) is endothermic whereas the encapsulation of O_2 (triplet) in C_{60} giving $O_2@C_{60}$ (triplet) at the DFT M06-2X/6-311g(d) level is an energetically favourable.

Table 2.8: Stabilization energy (in kcal/mol) of $Ge_2@C_{60}$ (singlet) with respect to Ge_2 (triplet) and C_{60}

Method	Basis Set	D_{5d}	D_{3d}	D_{2h}	C_{2h}
HF	6-311G(d)	189.42	189.44	188.99	189.20
B3Pw91	6-311G(d)	89.89	95.75	90.81	91.74
M06-2X	6-311G(d)	86.33	89.84	87.08	86.41
M06-L	6-311G(d)	58.58	65.28	61.98	58.37
	cc-pvtz	60.08	66.88	63.16	-

Table 2.9: Stabilization energy (in kcal/mol) of $Ge_2@C_{60}$ (triplet) with respect to Ge_2 (triplet) and C_{60}

Method	Basis Set	D_{5d}	D_{3d}	D_{2h}	C_{2h}
HF	6-311G(d)	190.20	189.45	188.73	189.13
B3Pw91	6-311G(d)	90.95	91.91	90.87	90.02
M06-2X	6-311G(d)	81.83	82.19	81.61	80.80
M06-L	6-311G(d)	61.79	63.38	63.26	60.57
	cc-pvtz	62.79	64.35	64.11	61.36

'-' represents convergence problem

Tables 2.8 and 2.9 give the stabilization energy values of Ge_2 triplet encapsulated in C_{60}. Clearly, Ge_2 encapsulation is always an endothermic process at all level of calculations. The relative instability found using DFT methods are much lower than that found using HF level of calculations. The probable reason is the electron correlation and dispersion interaction occurring between encapsulated Ge_2 and fullerene cage is incorporated in DFT methods. The stabilization energy obtained from M06 functionals is substantial, (~ 20 kcal/mol) indicating that the dispersion interaction between the ground state diatomic B_2 and O_2 and the cage is substantial.

2.3.4 Bond parameters and relative stability of encapsulated triplet over encapsulated singlet

Tables 2.10, 2.11 and 2.12 report the relative energy of the encapsulated triplet state with respect to the encapsulated singlet state. For $O_2@C_{60}$, the relative energy of encapsulated triplet state is similar to that of relative energy of O_2 triplet and O_2 singlet when it is free. The energy difference is negligible. This shows that the interaction of O_2 with the cage is same in triplet and singlet state. In the case of $B_2@C_{60}$, it was found that the energy difference between $B_2@C_{60}$ (triplet) and $B_2@C_{60}$ (singlet) is slightly higher in magnitude, suggesting that the triplet state is slightly stabilized inside the cage, when compared to the free B_2.The relative triplet-singlet energies of $Ge_2@C_{60}$ show a dependence on the orientation of Ge_2 in C_{60}, unlike $O_2@C_{60}$ and $B_2@C_{60}$. All levels of calculations show that the energy difference between the triplet and the singlet $Ge_2@C_{60}$ is less when compared to energy difference between the free Ge_2 triplet and singlet states. However, the magnitude of the energy differences is method dependent. The HF/6-311G(d) level of calculation suggests that the

singlet $Ge_2@C_{60}$ is slightly more stable than the triplet for D_{5d} orientation whereas the triplet is more stable than singlet for D_{2h} orientation. The energies of singlet and triplet are comparable for D_{3d} and C_{2h} orientations. DFT methods, which incorporate electron correlation show slightly different results. All DFT methods, except M06-2X method suggest that $Ge_2@C_{60}$ is more stable in the singlet state for D_{5d} orientation and the triplet state is more stable for the D_{3d} orientation. There is a spin cross over as Ge_2 rotates from D_{5d} to D_{3d} orientation. The spin cross over is observed in Ge_2 but not in B_2 and O_2 presumably because of the longer bond length of Ge_2, which enables it to interact with the inner wall of C_{60}. The electron density being different around a hexagonal ring compared to a pentagonal ring, gives rise to different interactions for these two different orientations. At the M06-2X level of calculation, the triplet is always more stable than the singlet and there is no spin cross over.

Table 2.10: Stabilization energy (in kcal/mol) of $B_2@C_{60}$ (triplet) with respect $B_2@C_{60}$ (singlet) for different orientations inside C_{60}

Method	Basis Set	D_{5d}	D_{3d}	D_{2h}	C_{2h}
HF	6-311G(d)	-31.62	-31.59	-31.63	-31.57
B3Pw91	6-311G(d)	-23.95	-23.94	-23.92	-24.06
M06-2X	6-311G(d)	-27.88	-28.24	-28.08	-28.17
M06-L	6-311G(d)	-29.30	-29.40	-28.94	-29.26

Table 2.11: Stabilization energy (in kcal/mol) of $O_2@C_{60}$ (triplet) with respect to $O_2@C_{60}$ (singlet) for different orientations inside C_{60}

Method	Basis Set	D_{5d}	D_{3d}	D_{2h}	C_{2h}
HF	6-311G(d)	-52.98	-52.99	-53.01	-53.00
B3Pw91	6-311G(d)	-38.73	-39.21	-39.30	-39.09
M06-2X	6-311G(d)	-37.36	-37.55	-37.73	-37.03

Table 2.12: Stabilization energy (in kcal/mol) of $Ge_2@C_{60}$ (triplet) with respect to $Ge_2@C_{60}$ (singlet) for different orientations inside C_{60}

Method	Basis Set	D_{5d}	D_{3d}	D_{2h}	C_{2h}
HF	6-311G				
	6-311G(d)	0.78	0.01	-0.26	-0.06
B3Pw91	6-311G(d)	1.06	-3.83	0.06	-1.72
M06-2X	6-311G(d)	-4.48	-7.65	-5.45	-5.61
	cc-pvtz	-4.45	-8.74	-	-
M06-L	6-311G(d)	3.21	-1.89	1.28	-0.93
	cc-pvtz	2.71	-2.25	0.95	-

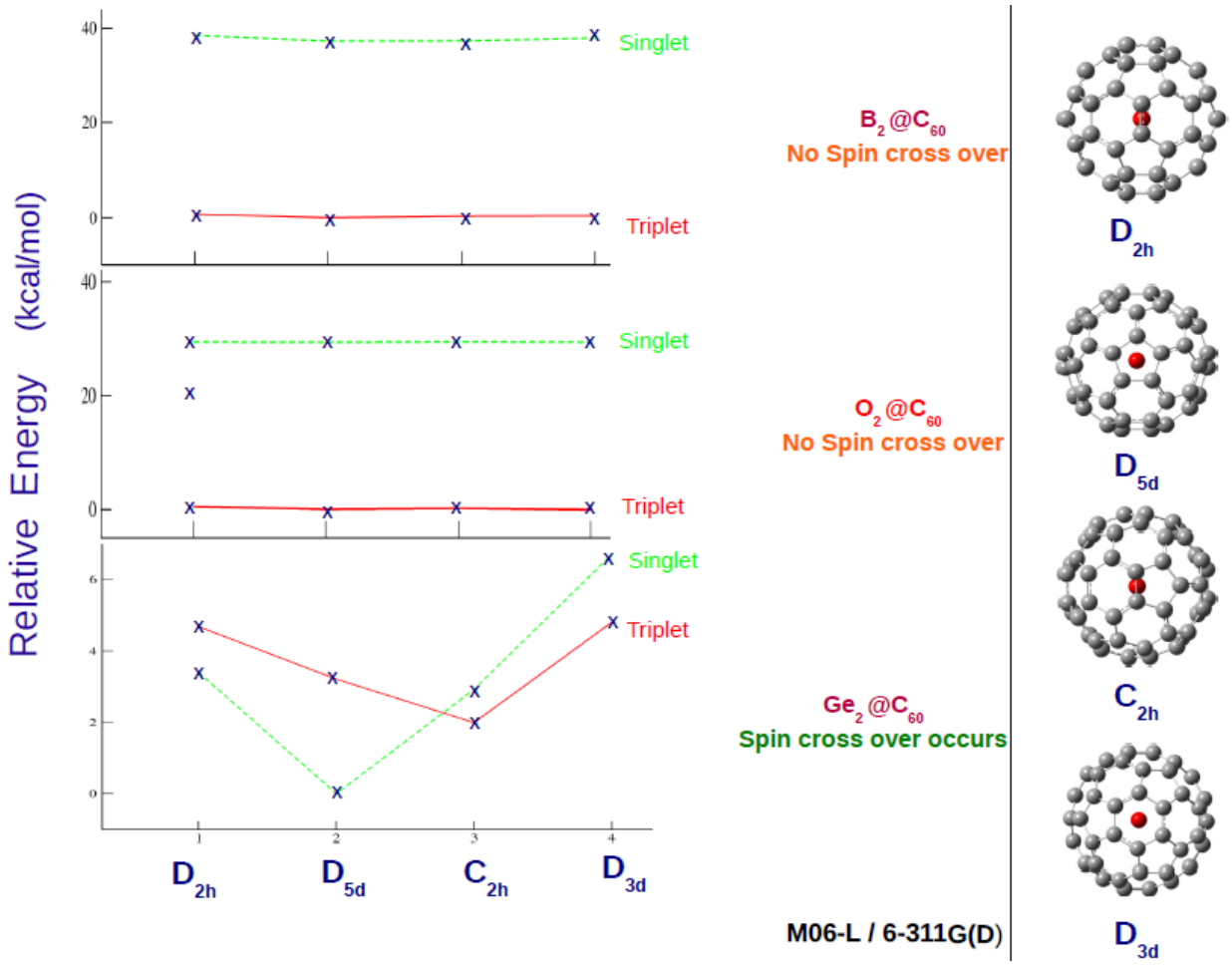

Figure 2.3: The relative energies of singlet and triplet states of $B_2@C_{60}$, $O_2@C_{60}$ and $Ge_2@C_{60}$ at the M06-L/6-311G(d) level of calculation.

2.3.5 Molecular orbital analysis

Tables 2.13 to 2.21 give the HOMO-LUMO energy gap for C_{60} and $X_2@C_{60}$ at different orientations and different methods. C_{60} molecule has a HOMO-LUMO energy gap of ~170 kcal/mol at the HF level of theory. At the DFT/B3Pw91/6-311g(d) level, the difference is 63 kcal/mol whereas at the DFT/M06-2X/6-311g(d) and DFT/M06-L/6-311g(d) levels of theory, the differences are ~103 kcal/mol and ~43 kcal/mol, respectively. At all levels of calculations, the HOMO is penta-degenerate while LUMO is triply degenerate.

Table 2.13: HOMO-LUMO energy gap(in kcal/mol) of C_{60} (singlet) at different levels of calculations

Method	Basis Set	Point group	HOMO-LUMO energy gap
HF	6-311G	I_h	172.89
	6-311G(d)	I_h	169.10
B3Pw91	6-311G(d)	I_h	63.22
M06-2X	6-311G(d)	I_h	104.02
	cc-pVTZ	I_h	103.84
M06-L	6-311G(d)	I_h	41.95
	cc-pVTZ	I_h	42.31

Tables 2.13, 2.14 and 2.15 list the HOMO-LUMO energy gap for $B_2@C_{60}$ in different orientations and for singlet and triplet states. Unrestricted spin was employed for calculation in the case of the triplet state and therefore alpha and beta sets of orbitals have different spatial energies. At the HF level of calculation, the HOMO-LUMO energy gap for $B_2@C_{60}$ for both singlet and triplet sates remains the same as that for C_{60}. In other methods, the singlet shows a lowering of the HOMO-LUMO gap, whereas for the triplet, the gap remains almost the same except for the M06-L method wherein for the alpha orbitals, the HOMO-LUMO gap reduces to ~33kcal/mol. Also, in the case of the singlet, the HOMO-LUMO gap decreases not because of any mixing of C_{60} and B_2 orbitals, but because of the fact that one or both of the HOMO and LUMO is contributed by B_2 which leads to a lowering of gap. (See Figure 2.4)

Table 2.14: HOMO-LUMO energy gap (in kcal/mol) of $B_2@C_{60}$ (singlet) for different orientations inside C_{60}

Method	Basis Set	D_{5d}	D_{3d}	D_{2h}	C_{2h}
HF	6-311G(d)	166.41	167.08	166.64	166.53
B3Pw91	6-311G(d)	29.87	30.01	30.05	29.93
M06-2X	6-311G(d)	78.39	78.82	78.84	78.65
M06-L	6-311G(d)	1.41	1.85	1.09	1.05

Table 2.15: HOMO-LUMO energy gap (in kcal/mol) of $B_2@C_{60}$ (triplet-alpha) for different orientations inside C_{60}

Method	Basis Set	D_{5d}	D_{3d}	D_{2h}	C_{2h}
HF	6-311G(d)	167.28	167.91	167.61	167.32
B3Pw91	6-311G(d)	60.91	61.34	61.53	61.1
M06-2X	6-311G(d)	100.10	100.74	100.93	100.29
M06-L	6-311G(d)	31.70	32.61	32.82	32.28

Table 2.16: HOMO-LUMO energy gap (in kcal/mol) of $B_2@C_{60}$ (triplet-beta) for different orientations inside C_{60}

Method	Basis Set	D_{5d}	D_{3d}	D_{2h}	C_{2h}
HF	6-311G(d)	167.22	167.85	167.58	167.30
B3Pw91	6-311G(d)	61.62	61.12	61.77	61.23
M06-2X	6-311G(d)	102.11	102.84	102.59	102.40
M06-L	6-311G(d)	40.41	40.90	40.73	40.51

$O_2@C_{60}$ (triplet) also does not show any change in HOMO-LUMO energy gap for all the orientations at all levels of theory whereas the singlet shows a lowering of energy gap at the DFT level, similar to $B_2@C_{60}$ singlet. Just like the $B_2@C_{60}$ sinlget, $O_2@C_{60}$ also shows contribution in HOMO or LUMO coming from O_2 molecule but no mixing of orbitals of fullerene cage and O_2 molecule (see Figure 2.5).

Table 2.17: HOMO-LUMO energy gap (in kcal/mol) of $O_2@C_{60}$ (singlet) for different orientations inside C_{60}

Method	Basis Set	D_{5d}	D_{3d}	D_{2h}	C_{2h}
HF	6-311G(d)	168.73	168.77	168.74	168.70
B3Pw91	6-311G(d)	17.78	17.02	16.57	17.21
M06-2X	6-311G(d)	80.89	80.90	80.87	81.31

Table 2.18: HOMO-LUMO energy gap (in kcal/mol) of $O_2@C_{60}$ (triplet-alpha) for different orientations inside C_{60}

Method	Basis Set	D_{5d}	D_{3d}	D_{2h}	C_{2h}
HF	6-311G(d)	168.69	168.82	168.77	168.70
B3Pw91	6-311G(d)	62.76	62.78	62.83	62.78
M06-2X	6-311G(d)	103.49	103.52	103.67	103.54

Table 2.19: HOMO-LUMO energy gap (in kcal/mol) of $O_2@C_{60}$ (triplet-beta) for different orientations inside C_{60}

Method	Basis Set	D_{5d}	D_{3d}	D_{2h}	C_{2h}
HF	6-311G(d)	168.74	168.83	168.78	168.74
B3Pw91	6-311G(d)	58.19	58.01	58.07	58.08
M06-2X	6-311G(d)	103.49	103.56	103.63	103.53

Table 2.20: HOMO-LUMO energy gap (in kcal/mol) of $Ge_2@C_{60}$ (singlet) for different orientations inside C_{60}

Method	Basis Set	D_{5d}	D_{3d}	D_{2h}	C_{2h}
HF	6-311G	130.89	130.06	130.87	129.88
	6-311G(d)	125.65	125.38	124.89	125.21
B3Pw91	6-311G(d)	28.61	21.81	26.09	25.52
M06-2X	6-311G(d)	64.59	56.38	59.23	57.90
	cc-pvtz	60.38	52.53	-	-
M06-L	6-311G(d)	10.21	5.94	6.63	-
	cc-pvtz	10.42	6.17	7.34	-

Table 2.21: HOMO-LUMO energy gap (in kcal/mol) of $Ge_2@C_{60}$ (triplet-alpha) for different orientations inside C_{60}

Method	Basis Set	D_{5d}	D_{3d}	D_{2h}	C_{2h}
HF	6-311G	93.68	94.76	95.58	94.40
	6-311G(d)	95.83	96.13	97.28	96.38
B3Pw91	6-311G(d)	19.60	32.02	20.69	20.64
M06-2X	6-311G(d)	47.73	48.05	48.26	48.59
	cc-pvtz	47.84	48.27	-	-
M06-L	6-311G(d)	3.59	4.25	4.79	4.44
	cc-pvtz	3.73	4.44	4.93	4.73

Table 2.22: HOMO-LUMO energy gap (in kcal/mol) of $Ge_2@C_{60}$ (triplet-beta) for different orientations inside C_{60}

Method	Basis Set	D_{5d}	D_{3d}	D_{2h}	C_{2h}
HF	6-311G	145.02	144.77	144.91	145.39
	6-311G(d)	140.61	140.30	140.32	140.66
B3Pw91	6-311G(d)	27.58	19.97	27.34	28.38
M06-2X	6-311G(d)	65.39	64.34	65.07	65.15
	cc-pvtz	62.55	62.51	-	-
M06-L	6-311G(d)	7.30	6.27	6.29	7.18
	cc-pvtz	8.54	7.97	7.15	8.78

In the case of $Ge_2@C_{60}$, the HOMO-LUMO energy gap decreases for both singlet and triplet states of $Ge_2@C_{60}$ compared to C_{60} which is attributed to the mixing of orbitals of both Ge_2 and fullerene cage (see Figure 2.6). Unlike $B_2@C_{60}$ and $O_2@C_{60}$, the HOMO-LUMO energy gap of $Ge_2@C_{60}$ shows orientational dependence. For singlet D_{5d} orientation, the gap is larger compared to other orientation.

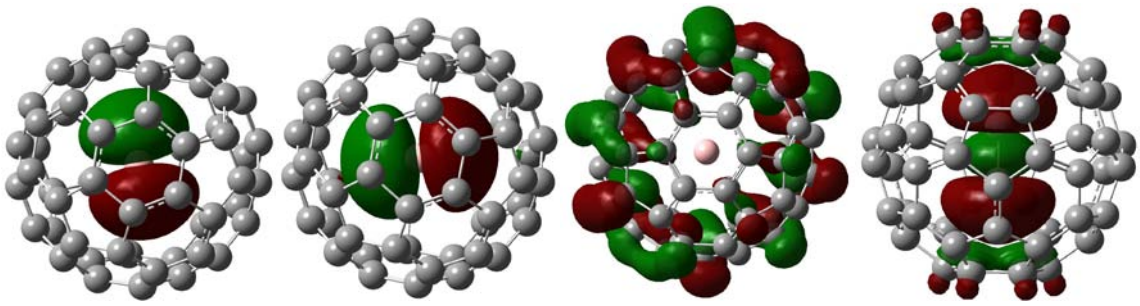

(a) **(b)** **(c)** **(d)**

Figure 2.4: (a) HOMO and (b) LUMO of $B_2@C_{60}$ (singlet) respectively. (c) HOMO and (d) LUMO of $B_2@C_{60}$ (triplet)

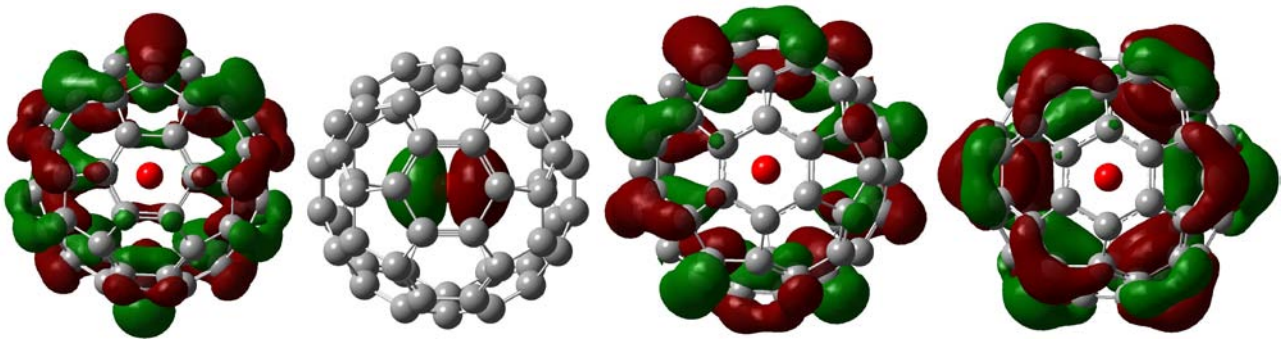

(a) **(b)** **(c)** **(d)**

Figure 2.5: (a) HOMO and (b) LUMO of $O_2@C_{60}$ (singlet) respectively. (c) HOMO and (d) LUMO of $O_2@C_{60}$ (triplet)

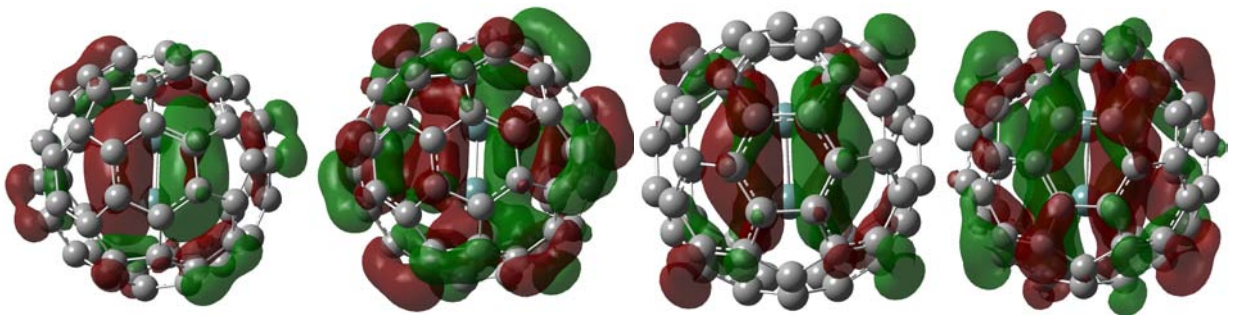

(a) **(b)** **(c)** **(d)**

Figure 2.6: (a) HOMO and (b) LUMO of $Ge_2@C_{60}$ (singlet) respectively. (c) HOMO and (d) LUMO of $Ge_2@C_{60}$ (triplet)

CHAPTER-3

3.1 Prismane formation

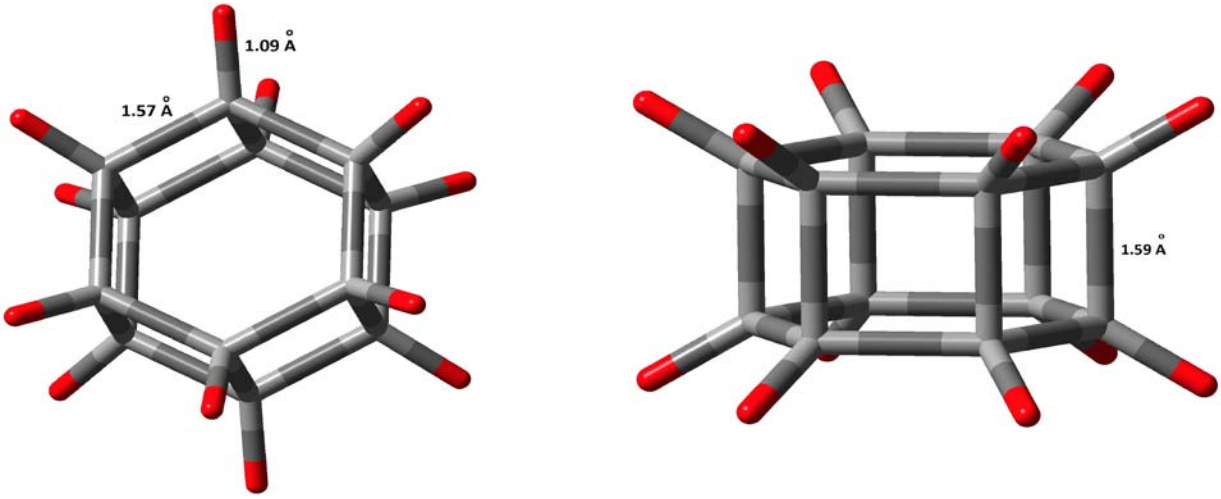

Figure 3.1: Top and side view of [6]-prismane

[n]-Prismanes are polycyclic hydrocarbons consisting of an even number of methine units and are of general formula $(CH)_{2n}$ that belong to the D_{nh} point group. Conceptually, the prismane structure was proposed by Ladenburg [32] as a structure for benzene $(C3H3)_2$, but the first practical realization of a prismane was achieved only in 1964 by Eaton and Cole [33] through their seminal efforts culminating in the synthesis of [4]-prismane (2, cubane). Since then, [3]-prismane and [5]-prismane have been synthesized. For a long time the synthetic process of [6]-Prismane was not deciphered until Mehta [34] came up with a novel idea to synthesize it. [6]-prismane is made up of twelve identical methine units $(CH)_{12}$ arranged at the corners of a regular hexagonal prism and the two parallel 6-membered rings are face-to-face co-joined by six 4-membered rings (see Figure 3.1). It is formally a face-to-face dimer of benzene. Many synthesized as well as theoretically predicted benzene dimers have been reported in the literature. A recent study by Hoffmann et al [35] discusses twelve benzene dimers, among which four are reported for the first time. Their calculations at the MP2/ccpvtz level of theory for the benzene dimers featuring one or more cyclohexadiene rings emphasize an instability of 50-99 kcal/mol in relation to two isolated benzene molecules. Prismane differs from the other benzene dimers due to the absence of cyclohexadiene rings and there are no unsaturated carbon atoms. Ab initio calculations using the MP2/ccpVTZ method suggest D_{6h} symmetry as the lowest energy arrangement for hexaprismane with a steric energy of 115 kcal/mol

(MP2/ccpvtz) with respect to two isolated benzene molecules, indicating that [6]-prismane is the least stable benzene dimer. Figure 1.0 enlists the twelve benzene dimers mentioned by Hoffmann et al.

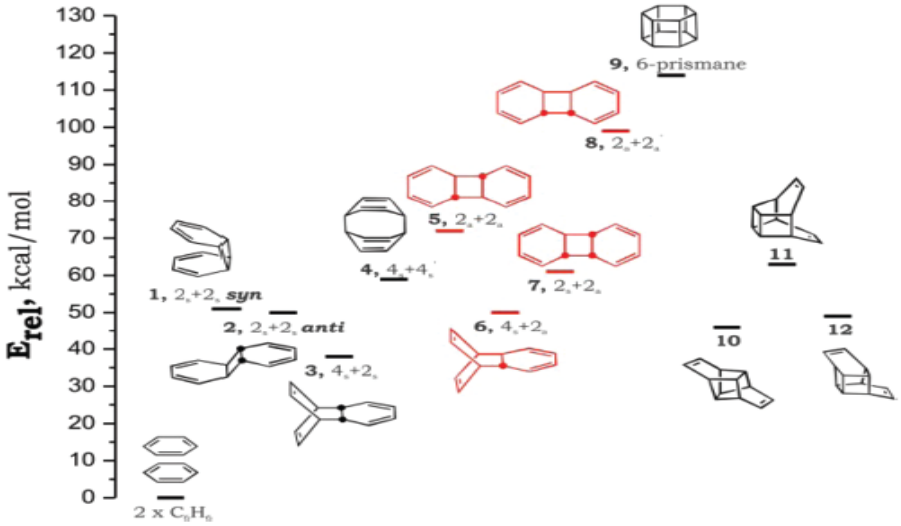

Figure 3.2: Relative energies of different benzene dimers

Although carbon and silicon belong to the same group in the periodic table, there exists a significant difference in their bonding abilities. Many unsaturated carbon compounds exist but unsaturated silicon compounds are rare as silicon prefers an sp^3 bonding environment over sp^2 hybridization. However, a few recent publications report that multiple bonds between Si are possible [36]. Compounds containing Si=Si bonds are now known. Dutta [35] has studied the structural properties of a series of silicon substituted benzenes ($C_nSi_mH_6$), where n varies from 0 to 6 and m = (6-n). Three isomers (1,2), (1,3) and (1,4) of disilabenzene are possible for doubly silicon substituted benzene. All three of them are planar. (1,2) and (1,3) disilabenzene are lower in energy than (1,4) disilabenzene. For a tri-silicon substitution, there are three possible isomers, (1,2,3), (1,2,4) and (1,3,5) trisilabenzene. Among these, (1,3,5) trisilabenzene, the lowest energy isomer is planar, while the other two are non-planar. Three isomers are possible for a tetra-substituted benzene. They are (1,2,3,4), (1,2,3,5) and (1,2,4,5) tetrasilabenzene . Out of these, (1,2,3,5) tetrasilabenzene is the most stable. The detailed electronic structure of all these isomers is elucidated in Dutta's paper [37]. These silicon substituted benzenes have Si=Si bonds and they exhibit a pseudo-Jahn-Teller distortion (PJT) due to which three Si atoms in conjugation undergo puckering/buckling to have a sp^3 hybridization. PJT is attributed to the sufficiently strong coupling between the unoccupied orbitals and the occupied molecular orbitals. Silicenes have a smaller HOMO-LUMO energy gap than their carbon counterparts, which leads to a stronger orbital coupling. This is the reason why

PJT is observed in unsaturated silicon compounds but not in carbon compounds. Dutta's paper [38] elucidates the buckling in silicenes in detail. An analysis of σ-π separation in Si_6H_6 using natural energy decomposition analysis (NEDA) suggests that the σ backbone is stabilized, whereas the π backbone is destabilized due to buckling. However, the stabilization of buckled σ backbone overwhelms the π backbone destabilization thus explaining why buckled Si_6H_6 is more stable than planar Si_6H_6. This is contrary to what happens in graphene/benzene due to which graphene/benzene prefers to be in a planar form over the puckered form. Our calculations also show that the optimized geometry of Si_6H_6 exhibits a puckered structure with a puckering angle of 35^o. The planar structure of Si_6H_6 is not a minimum energy isomer. It is a first order saddle point and is 9.2 kJ/mole higher in energy than the puckered Si_6H_6. The puckered form belongs to D_{3d} point group. As explained earlier, the additional stability of the puckered form is accounted for by σ-π mixing, which is allowed because of puckering. Figure 2 illustrates the geometry of sequentially silicon substituted benzenes.

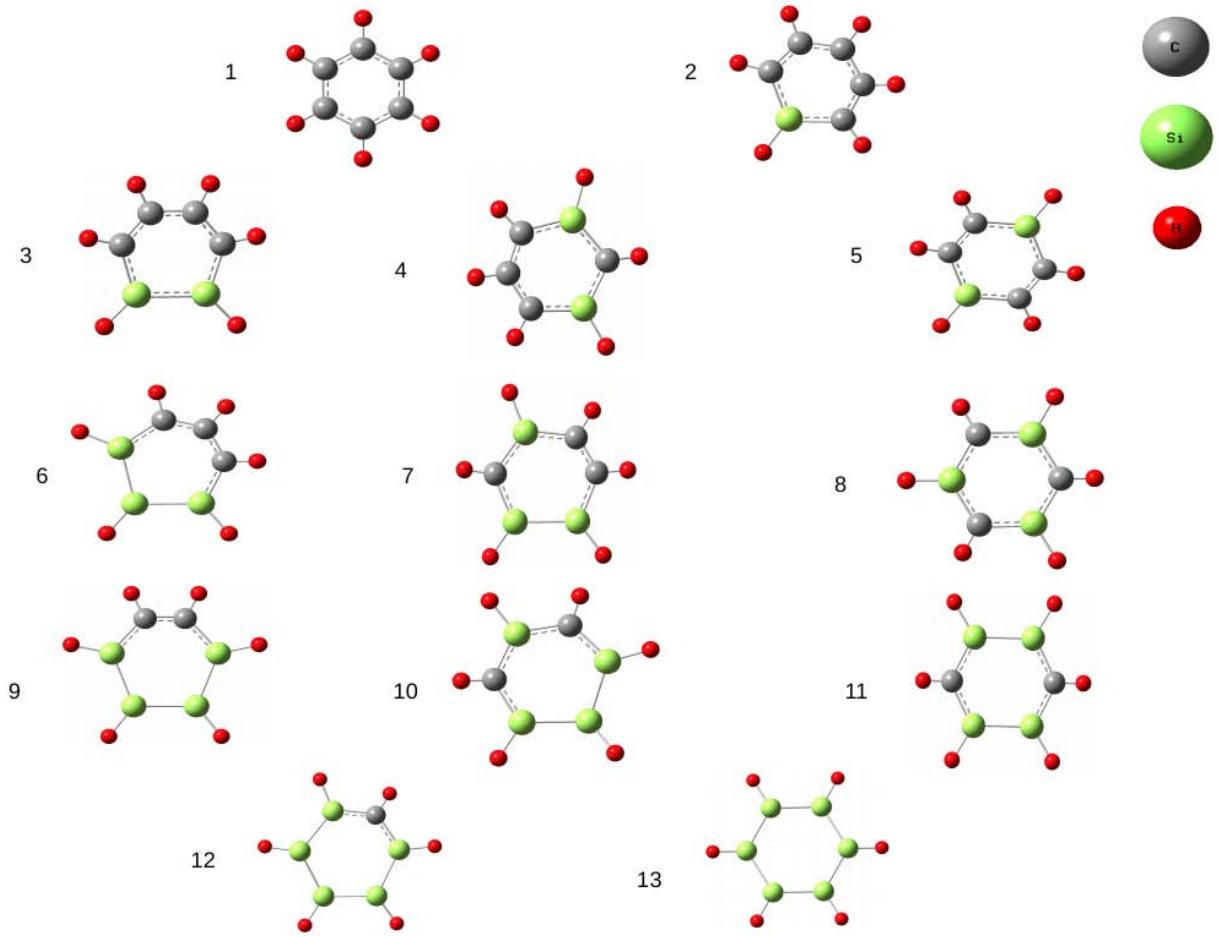

Figure 3.3: The geometry of Si-substituted benzene

Theoretical calculations done by us show that [6]-prismane made up of silicon substituted benzene,

Si_6H_6 is stable with respect to the monomers. To get a better understanding of why hexaprismane formed by two benzene units is relatively unstable whereas the one formed by hexasilabenzene units is stable, we have sequentially substituted each carbon of benzene with silicon and compared the stability of two isolated monomers with the prismane of the Si-substituted benzene. The minimum energy structure for benzene, silicon substituted benzenes and their dimers was found using the MP2 method and the double zeta basis set, using Gaussian09 suite of programs [36]. Frequency calculations were also carried out to ensure that all the optimized geometries obtained correspond to true minima.

3.2 Results and Discussion:

The Si-Si bond length in the optimized geometries of the dimers of substituted benzene varies from 2.28 Å to 2.45 Å, whereas the C-C bond length in the substituted benzene varies from 1.5 to 1.65 Å. Natural bond orbital analysis showed a 26% s character and 74 % p character in the C-C bond of the substituted benzene ring, whereas a higher p (~76%) character and a lesser s character was found in the bond between the C atoms joining the two benzene rings. Similarly, the p character in the Si-Si planar bond is less than that in the Si-Si bond formed between layers. C-Si bonds are polarized with C having more than 70% share of the electrons. Likewise, the Si-H bond is also slightly polar with the H atoms being the more electronegative and having a share of almost 60% of the bond electrons. The energy of the dimer was compared with the energy of the corresponding two isolated monomers (substituted benzene). The structure of the silicon substituted benzene is reproduced in Figure 3.3. Dimers are shown in Figure 3.4.

The dimer formed by covalent interaction between two benzene rings is unstable when compared to two isolated benzene rings by an energy of 130 kcal/mol. In benzene, each carbon is bonded to other atoms with three σ bonds which are sp^2 hybridized and one π bond, which has pure p character. When the dimer is formed, each carbon forms four σ bonds as a result of covalent interaction. σ bonds are generally more stable than π bonds and hence the formation of [6]-prismane is expected to be energetically favorable. But electronic structure calculations predict that the covalently bonded benzene dimer is unstable. The reason for the instability is the formation of six 4-membered planar cyclobutane rings. Planar cyclobutanes are unstable because of ring strain. The resonance energy of benzene is 36kcal/mol, which is also lost with the formation of prismane. Therefore, the stability gained by the formation of σ bond is offset by the formation of planar cyclobutane rings and loss of aromaticity.

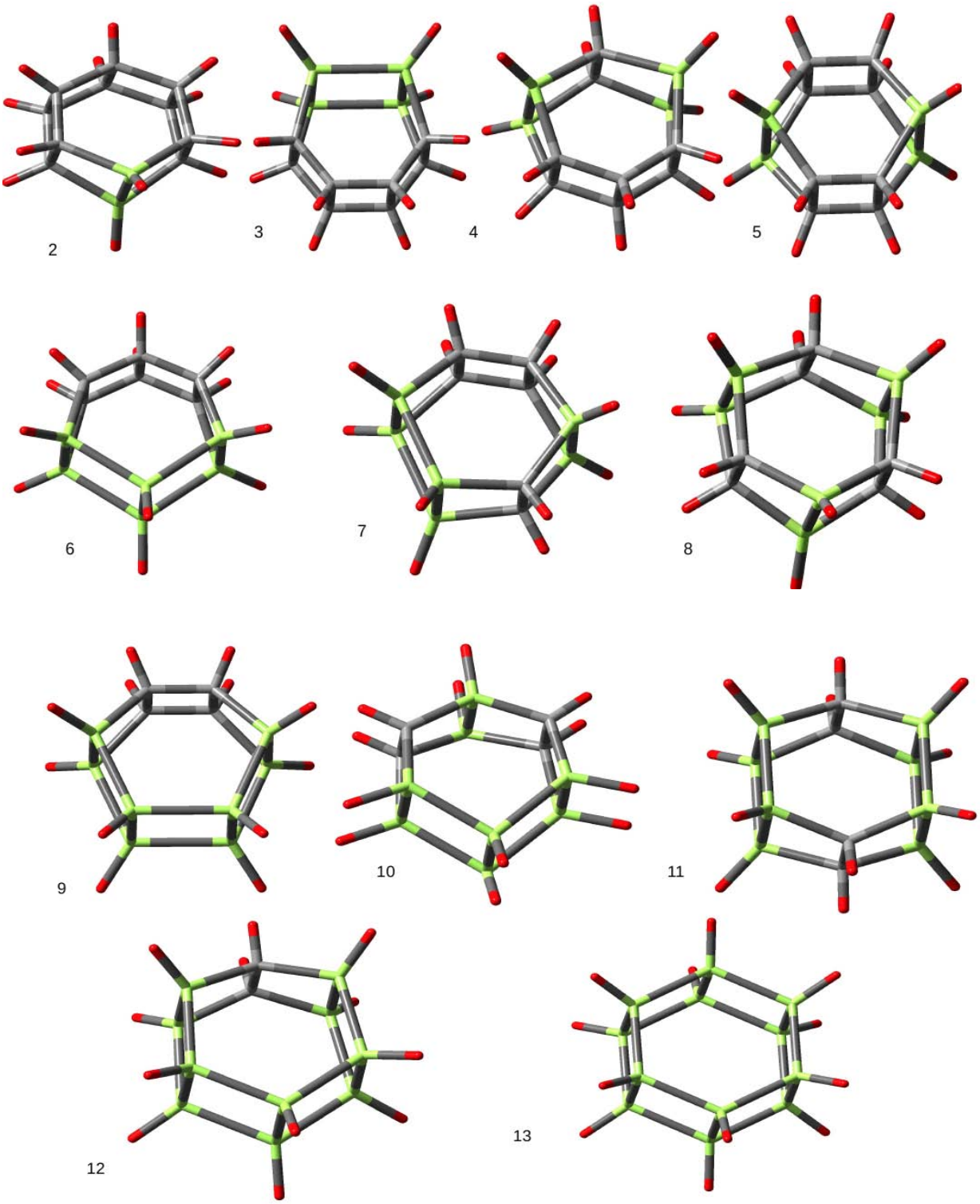

Figure 3.4: The optimized geometry of the different dimmers of substituted benzene moeity

In the case of singly substituted benzene also, the dimerization is expected to be favored because of

the formation of six σ bonds between the monomers. Among the six sigma bonds, there is a Si-Si σ bond between the monomers. It gives a sp^3 bonding environment to silicon. Yet the dimer formed by single silicon substituted benzene is unstable by an energy of ~50 kcal/mol, due to the formation of four planar cyclobutane rings, that are strained.

For a multi-Si-substituted benzene, the stability of the dimer depends on the position of Si substitution in the benzene ring. In the case of doubly substituted benzene ring, the dimer formed by (1,2) disilabenzene is slightly unstable as it leads to the formation of three cyclobutane rings, whereas those formed by (1,3) and (1,4) disilabenzene are stable as they lead to the formation of only two cyclobutane rings. Among these two dimers of doubly substituted benzene, (1,4) disilabenzene is more stable as the two cyclobutane rings are separated from each other. However, in (1,3) disilabenzene, the cyclobutane rings are juxtaposed to each other. (1,3) and (1,4) disilabenzene are stabilized by ~9kcal/mol with respect to their monomers.
For a triply substituted benzene, three Si-Si σ bonds are formed and hence the stability of the dimer is more compared to the dimer of doubly substituted benzene. Among different isomers of tri-substituted benzene, (1,2,3) trisilabenzene dimer is the least stable as it has two cyclobutane rings and (1,3,5) is more stable as no cyclobutane ring is formed.

For a tetra-substituted benzene ring, dimerization is preferred. (1,2,3,5) tetrasilabenzene dimer is the most stable as it has no cycylobutane ring and there are four Si-Si σ bonds. (1,2,3,4) tetrasilabenzene is the least stable as it has one cyclobutane ring. The relative stability of the dimer of (1,2,3,5) tetrasilabenzene with respect to the two monomers is +84 kcal/mol.

Penta subtituted silabenzene forms a stable dimer with a stabilization energy equal to 112 kcal/mol. In this dimer, there are no cyclobutanes rings formed. Hexasilabenzene forms the most stable dimer/prismane and the stability with respect to the two monomers is 134 kcal/mol. It has D_{6h} symmetry with six covalent Si-Si σ bonds between the rings. In the case of silicon substituted benzene dimer, it was observed that the stability of the dimer increases with an increase in the number of Si atoms. Table 3.1 & Figure 3.5 show the relative stability of dimers formed as a function of the number of carbon atoms.

Table 3.1: Relative stability of the dimer with respect to the two asymptotically monomers of

benzene and different Si-substituted benzene at the MP2/cc-pVDZ level of theory

$C_nSi_{(6-n)}H_6$	Symmetry of dimer	ΔE
C_6H_6	D_{6h}	135.12
$C_5S_1H_6$	C_{2h}	42.96
(1,2) $C_4S_2H_6$	C_{2V}	0.48
(1,3) $C_4S_2H_6$	C_{2V}	-10.58
(1,4) $C_4S_2H_6$	D_{2h}	-21.78
(1,2,3)$C_3S_3H_6$	C_{2V}	-38.83
(1,2,4) $C_3S_3H_6$	C_S	-54.44
(1,3,5) $C_3S_3H_6$	D_{3h}	-48.35
(1,2,3,4) $C_2S_4H_6$	C_{2V}	-79.25
(1,2,3,5) $C_2S_4H_6$	C_S	-84.05
(1,2,4,5) $C_2S_4H_6$	D_{2h}	-88.37
$C_1S_5H_6$	C_{2V}	-112.65
Si_6H_6	D_{6h}	-134.83

$\Delta E_{stab} = (E_{Di} - 2 * E_{mono})$ (kcal/mol)

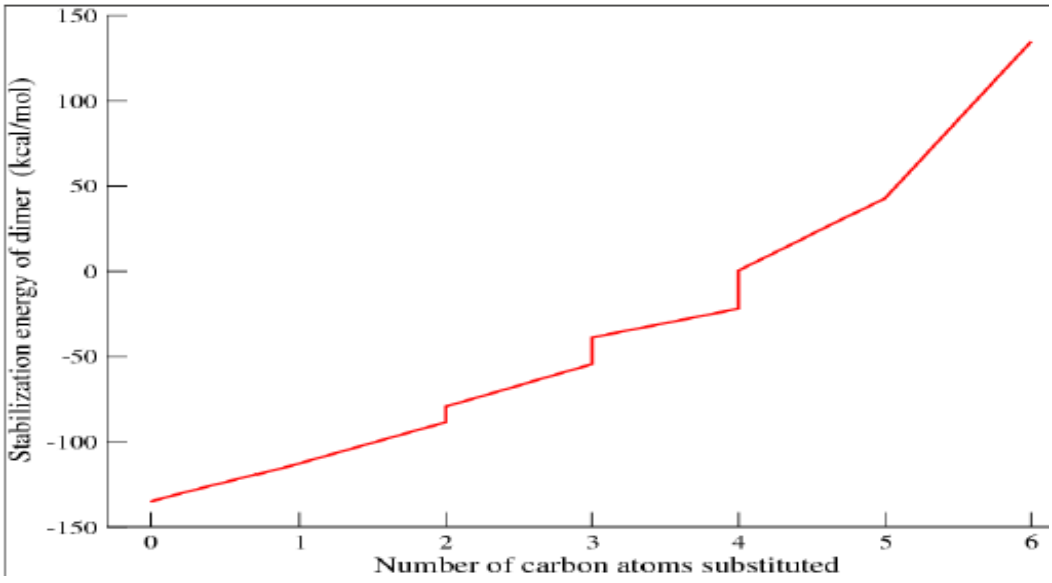

Figure 3.5: Relative stability of the dimer with respect to the two asymptotically monomers of benzene and different Si-substituted benzene at the MP2/cc-pVDZ level of theory

Since Ge belongs to the same group as Si and C in the periodic table, we were curious to know the

stability of Ge-substituted benzene and its dimer. We repeated the same set of calculations for Ge-substituted benzene. It was found that planar Ge_6H_6 with D_{6h} point group symmetry is not a minimum energy structure, but a second order saddle point. Ge_6H_6 exists in a puckered form like Si_6H_6 and the cause can be attributed to the pseudo-Jahn-Teller effect as was explained by Dutta [39] in the case of Si_6H_6. The HOMO orbital of Ge_6H_6 is doubly degenerate and the LUMO is non-degenerate similar to the case of Si_6H_6. But the HOMO-LUMO energy gap in Ge_6H_6 is smaller by ~6.5 kcal/mol than that of Si6H6. This smaller HOMO-LUMO energy gap leads to a greater PJT effect and hence a larger distortion in the structure of Ge6H6. This is observed as an enhancement in the puckering angle from 34.65^o in Si_6H_6 to 46.64^o in the case of Ge_6H_6.

Ge-Ge bond length is slightly longer than Si-Si bond length in the optimized geometries of the dimers of substituted benzene. Ge-Ge bond length varies from 2.4 Å to 2.5 Å and C-C bond lengths are between 1.5 to 1.6 Å in the germanium substituted benzene dimer. A natural bond orbital analysis using the NBO 3.1 package revealed a 27.4 % s orbital character and 72.5 % p orbital character in the C-C bond present in the ring in comparison to 76% p character and less s character in the C-C bond present between two rings. Similarly, it was found that the p character in a Ge-Ge planar bond in a ring is less than that in the Ge-Ge bond joining the monomers. The Ge-Ge bond between layers has more than 78% contribution from p orbitals. C-Ge bonds are polarized with C having more than 72% electron share. C-Ge Bonding is sp^2 hybridized in both C and Ge. Ge-H is also slightly polar like Si-H. H is more electronegative than Ge, thus, accounting for H having a greater electron share of 59%.

Dimerization energy values for Ge-substituted benzene were calculated the way they were calculated for silicon substituted benzene. A trend similar to that observed for Si was observed for Ge. That is, on increasing the number of substituted Ge atoms, the stability of the dimer increased. For a single germanium substituted benzene, the dimer formation is energetically unfavorable by ~35 kcal/mol. For multi-Ge substituted benzene, the stability of the dimer, like for multi-Si substituted benzene, depends on the position of Ge substitution in the benzene ring. Vibrational frequency calculations show that (1,2) di-germanium benzene, (1,2,3) and (1,2,4) tri-germanium-benzene and (1,2,3,4) tetra-germanium-benzene are not minimum energy configurations but are saddle points. The calculations, however, show their dimers to be relatively stable. The dimers of (1,3) and (1,4) di-germanium benzene are stable by ~30 kcal/mol. The dimer formed by (1,3,5) tri-germanium benzene is relatively the most stable, with a stabilization energy of 80 kcal/mol. The stabilization energy due to dimerization in tetra-substituted benzene is 107 kcal/mol whereas in the case of penta-substituted germanium it increases to 120 kcal/mol. Hexa-germanium-benzene dimer

is the most stable of all Ge-substituted-benzene and its stabilization energy equals 132 kcal/mol. It is evident that the trends observed for Ge substituted benzene are similar to those observed in Si substituted benzene and thus can be explained in a similar manner

Prismane/dimer formation by fluorinated benzene and silicon substituted fluorinated benzene was also investigated. Fluorine, the most electronegative element in the periodic table, has an electron withdrawing effect. While perfluorobenzene C_6F_6 is planar with D_{6h} symmtery, other perhalobenzenes are non-planar, belonging to D_{3h} point group. As a result, the overlap between the p orbitals in C_6F_6 is large resulting in a higher aromaticity in C_6F_6. Fluorine behaves as an electronegative atom with respect to sigma electrons, but is electropositive with respect to π electrons. In hexafluorobenzene, fluorine withdraws electron density from carbon through sigma bonds but donates electrons to the pi orbitals of the carbon atom thereby increasing the aromaticity. A calculation of nucleus independent chemical shift (NICS) values has also predicted an increase in the aromaticity of fluorinated arene rings. Dimerization of hexafluorobenzene is facilitated by the addition of six sigma bonds. The electron density of the fluorine atom is increased in the dimer as back donation is not possible due to the absence of π electrons. NBO calculations show a 12 % enhancement in the electron density of fluorine atoms in the dimer when compared to the monomer. An increase in the electron density of the fluorine atoms leads to an increase in the stability.

The hexagonal rings of C_{60} fullerene have unsaturated carbons but are much less aromatic than benzene ring. We were interested in finding out the possibility/feasibility of formation of capped fullerene (see Figure 3.6). We found that capped fullerene can indeed be formed with six extra sigma bonds. This structure belongs to C_{3V} point group. The C-C bond length joining the fullerene cage and benzene is 1.56 Å, while the C-C bond in the cap has length of 1.55 Å. This capped fullerene structure is unstable by 101.27 kcal/mol, with respect to isolated benzene and fullerene molecules, at HF/ccpVDZ level of theory. It should be noted here that this energy is lower than the destabilization energy of two benzene molecules forming [6]-prismane, which is ~ 138 kcal/mol. In the case of prismane formation, the loss in aromaticity is large, whereas in a capped fullerene, only benzene loses its aromaticity.

Similar calculations were carried out for spherical Si_{60} capped with hexasilabenzene. It was found that the capped silicon-fullerene was stable with respect to isolated Si_{60} and Si_6H_6 by energy of ~134.kcal/mol. It should be noted that icosahedral Si_{60} is not an energy minimum but rather a first order saddle point. But some of the endohedral Si_{60} are stable.

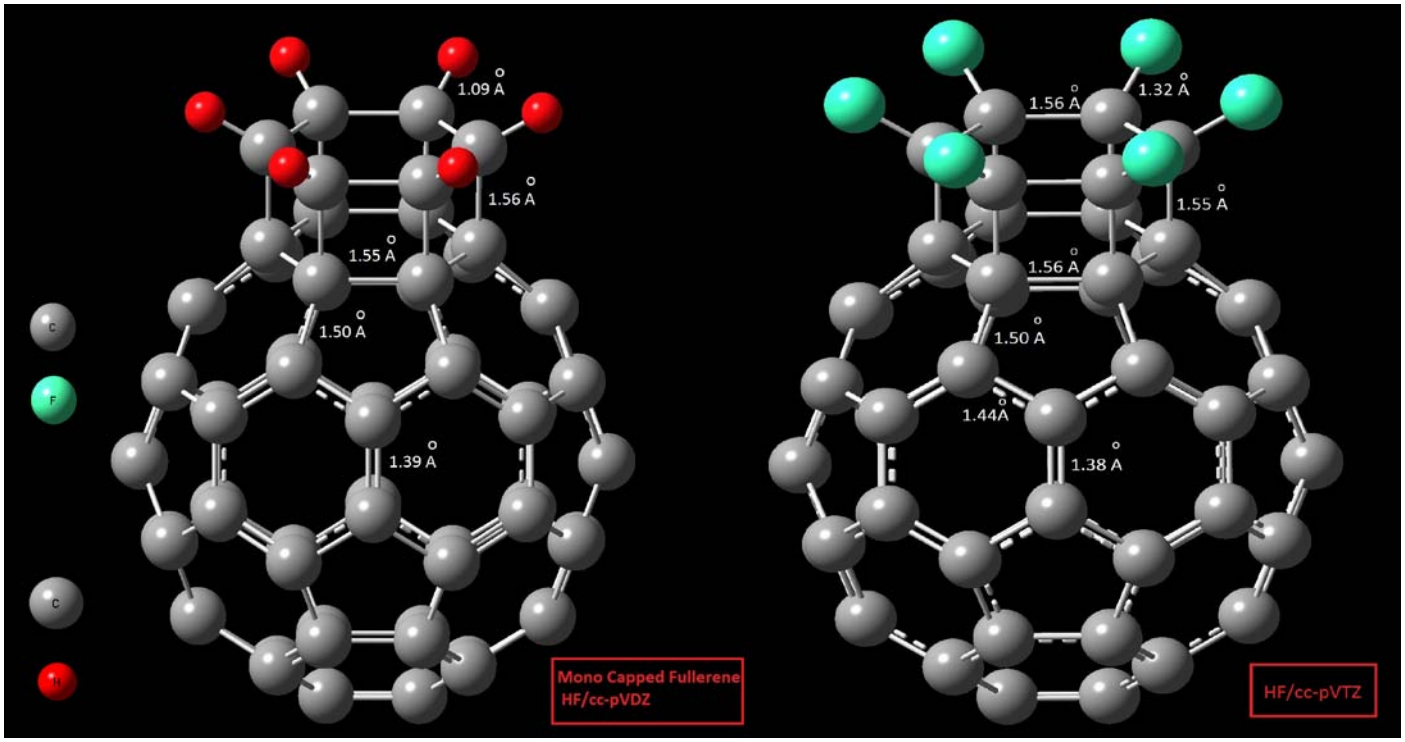

Figure 3.6: Capped fullerene

CHAPTER-4: Summary and Conclusion

Ab initio and DFT calculations have been carried out for $B_2@C_{60,}$ $O_2@C_{60}$ and $Ge_2@C_{60}$ to study the influence of the fullerene cage on the relative stability of the triplet and singlet states of the diatomic molecules.

For $O_2@C_{60}$, the relative energy of the encapsulated singlet and triplet states is similar to that of the relative energy of the singlet and triplet states of O_2 when it is free. In the case of $B_2@C_{60}$, it was found that the energy difference between $B_2@C_{60}$ (triplet) and $B_2@C_{60}$ (singlet) is slightly larger in magnitude, suggesting that the triplet state is slightly more stabilized inside the cage than in free B_2. However, the energy gap between the triplet and the singlet state of $Ge_2@C_{60}$ is significantly different from that that of free Ge_2 and it shows a dependence on the orientation of Ge_2 in C_{60}. All DFT calculations except the one using M06-2X suggest that $Ge_2@C_{60}$ is more stable in the singlet state in the D_{5d} orientation and the triplet state is more stable in the D_{3d} orientation. The electron density is different around a hexagonal ring when compared to a pentagonal ring in C_{60}, giving rise to different interactions for these two orientations.

There is a spin cross over as Ge_2 rotates from D_{5d} to D_{3d} orientation. No such spin cross over is observed in B_2 and O_2 presumably because they have shorter bond lengths and there is very little interaction between them and the inner wall of the cage.

In the case of silicon substituted benzene dimers, it was observed that the stability of the dimer increases with an increase in the number of Si atoms. This is presumably because with an increase in the number of Si atoms, the number of cyclobutane rings decreases and simultaneously there is an increase in the number of silicon atoms getting energetically favourable sp^3 hybridization. The trends observed for Ge-substituted benzene are similar to those observed for Si-substituted benzene.

Capped fullerenes are unstable when compared to isolated benzene and C_{60} fullerene. But the instability is less when compared to the instability of [6]-prismane. An increased stability of the capped fullerene is noticed, when the hydrogen atoms in the benzene ring are replaced by the more electronegative fluorine atoms.

Bibliography

[1] J. R. Heath, S.C. O'Brien, R.F. Q. Zhang, Y. Liu, R.F. Curl, H.W. Kroto, F.K. Tittel, R.E. Smalley, J. Am. Chem. Soc., **107**, 779 (1985)

[2] D.S. Bethune, R,D. Jhonson, J.R. Salem, M.S. de Vries, C.S. Yanoni, Naturr, **336**, 123 (1993)

[3] . K. Komatsu, M. Murata, Y. Murata, Science, **307**, 238 (2005)

[4] Cioslowski and E.D. Fleischmann, J. Chem. Phys., **116**, 10684 (2002)

[5] C.N. Ramachandran, N. Sathyamurthy, Chemical Physics Letters 461, 87 (2008)

[6] Lu, Z. Zhang, X.Zhao, Sol. State Comm., **110**, 565 (1999)

[7] J.M. Park, P. Tarakeshwar, K.S. Kim, J. Chem. Phys., **116**, 10684 (2002)]

[8] A.D. Buckingham, J.P. Read, Chem. Phys. Lett., **253**, 414 (1996)

[9] J.Lu, W.N. Mei, Y.Gao, X. Zeng, M. Jing, G. Li, R. Sabirianow, Z. Gao, L. You, J. Xu, D. Yu, H. Ye, Chem. Phys. Lett., **425**, 82 (2006)

[10] R.J. Cross, J. Phys. Chem.A., 105, **6943** (2001)

[11] C. Zicovich, Atoms and molecules in cavities: A method for study of spatial confinement.

[12] A. Borgoo, D. J. Tozer, P. Geerlings, F. De Proft, Phys. Chem. Chem. Phys., **10,** 1406 (2008)

[13] R.B. Ross, C.M. Cardona, D.M. Guldi, S.G. Sankaranarayanan, M.O. Reese, N. Kopidakis, J.Peet, B.Walker, G.C. Bazan, E. V. Keuren, B.C. Holloway, M.Drees, Nature Materials **8,** 208 (2009)

[15] O. Shameema, C.N. Ramachandran, N.Sathyamurthy, J. Phys. Chem. A. Lett., **110,** 2 (2006)

[16] C.N. Ramachandran, N.Sathyamurthy, Chem. Phys. Lett., **410**, 348 (2005)

[17] Ira N. Levine, Quantum Chemistry (7th Edition)

[18] H.W. Kroto, J. R. Heath, S.C. O'Brien, R.F. Curl, R.E. Smalley, Nature, **318**, 162 (1985)

[19] K. A. Affholter,S .J. Henderson, G.D. Wignall, G.J. Bunick, R.E. Haufler,R.N. Compton,J.Chem. Phys. **99,** 9224 (1993)

[20] R.E. Smalley Acc. Chem. Res., Vol. 25, No. 3

[21] K. H. Ang, I. Alexandrou, N. D. Mathur, G. A. J. Amaratunga, S Haq, *Nanotechnology* **15**, 520 (2004)

[22] O. *Müller*, R. Herbst-Irmer, L. N. Markovskii, Y. G. Shermolovich,synthesis metals **103** (1993) 2417-2418

[23] P. R. Bandaru, J.Nanoscience and Nanotechnology Vol.7, 1–29, 2007

[24] J. M. Bronard, A. Sallin, EPFL, Lausane, Switzerland

[25] B.N.di, A. Antal, A.P. Sztor, A. Ja nossy J. Phys. Chem. Lett. **3**, 3291, (2012)

[26] Lee, G. H.; Huh, S. H.; Jeong, J. W.; Ri, H.-C. J. Magn. and Magn. Mate., **246**, 404

[27] V.K. Koltover, Paramagnetic Endohedral Fullerenes pp 259 NOVA

[28] A. Krap, G. Frenking, Chem. Eur. J., **13**, 8256 (2007)

[29] X.Wu, X. Lu, J. Am. Chem. Soc., **129**, 2171 (2007)

[30] CCBDB experimental bond lengths, NIST database

[31] C.Clouthier, F. Grein, P.J. Bruna, Mole. Phys., **103**, 3253 (2005)

[32] A. Ladenburg, *Encyclopædia Britannica* , (12th ed.) (1922)

[33] F. Biegle-Koning, R. F. W. Bader, W. -H. Tang, *J. Comput. Chem.* , **96,** 6796 (2000)

[34] G.Mehta, Padma, *Tetrahedron*, **Vol4 1**(1991)

[35] A.Y.Rogachev, X.V.Wen, R.Hoffmann,J. Am. Chem. Soc. **134**, 8062−8065 (2012)
[36] S.Nagase, H.Teramae, T.Kudo, J. Chem. Phys., **86**, 45134517(1987)
[37] V. Mohan, A. Datta, J. Phys. Chem. Lett.1, **136**,(2010)

[38] D.Jose, A. Datta, J. Phys. Chem. C, **116**, 24639(2012)